

Spin Diffusion in the $S = 1/2$ Quasi One-Dimensional Antiferromagnet $\text{-VO}(\text{PO}_3)_2$ via ^{31}P NMR

Jun Kikuchi, Naohiko Kurata, Kiyochiro Motoya,
 Tetsu Yamauchi¹ and Yutaka Ueda¹

Department of Physics, Faculty of Science and Technology, Science University of Tokyo,
 2641 Yamazaki, Noda, Chiba 278-8510

¹Institute for Solid State Physics, University of Tokyo, 5-1-5 Kashiwanoha, Kashiwa, Chiba 277-8581

(Received February 15, 2001)

Low-frequency spin dynamics in the $S = 1/2$ antiferromagnetic spin-chain compound $\text{-VO}(\text{PO}_3)_2$ has been studied by means of ^{31}P NMR. The nuclear spin-lattice relaxation rate $1/T_1$ at the P site exhibits $\omega^{-1/2}$ dependence on the applied magnetic field (H) at temperatures (T) well above the intrachain coupling strength $J = k_B = 3.50$ K indicating one-dimensional diffusive spin dynamics. The diffusive contribution to $1/T_1$ decreases on cooling as electronic spins acquire short-range antiferromagnetic correlations within the chain, and vanishes almost entirely around $T = J = k_B$. This is accompanied by an apparent increase of the spin-diffusion constant from the value expected in the classical limit. On the other hand, the field-independent part of $1/T_1$ increases with decreasing temperature, which may be a precursor for the true long-range antiferromagnetic ordering found below $T_N = 1.93 \pm 0.01$ K.

KEYWORDS: $\text{-VO}(\text{PO}_3)_2$, NMR, antiferromagnetic spin chain, nuclear spin relaxation, spin diffusion

1. Introduction

There has been a continued interest in the dynamics of low-dimensional quantum antiferromagnets at finite temperatures. One of the issues which has attracted renewed attention is a problem of spin diffusion in the one-dimensional (1D) Heisenberg spin chain. It is argued from phenomenology that at high enough temperatures and at long times, the spin autocorrelation function of the 1D Heisenberg spin chain has a diffusive form

$$\langle S_i(t) S_i(0) \rangle \sim t^{-1/2}; \quad (1.1)$$

leading to divergence of the spectral density at low frequencies as $\omega^{-1/2}$. However, because the diffusive form (1.1) is not derived from the microscopic Hamiltonian but is a consequence of the hydrodynamical assumption for the spin-spin correlation,¹⁾ the question on the existence of spin diffusion in 1D spin chains has been studied intensively from both theoretical and experimental viewpoints. One of the best studied theoretical models is the $S = 1/2$ XXZ chain represented by the Hamiltonian^{2,3,4,5,6,7)}

$$H = J \sum_i (S_i^x S_{i+1}^x + S_i^y S_{i+1}^y + S_i^z S_{i+1}^z); \quad (1.2)$$

At the isotropic point ($\Delta = 1$) and at low enough temperatures ($T \ll J = k_B$), analytical expressions for the dynamical susceptibility (χ'') have been derived for $q = 0$ and $q = \pi$, and are shown to have no diffusive pole at low frequencies.²⁾ At modestly high, or much higher temperatures compared with the intrachain coupling strength J , the problem is still controversial. Although the absence

of diffusive excitations seems to be settled for the XXZ chain with planar anisotropy ($0 < \Delta < 1$), a definite answer for the absence (or presence) of spin diffusion at the isotropic point has not yet been given.

Diffusive behavior of the spin-spin correlation has been observed experimentally in several 1D spin chains via the $\omega^{-1/2}$ resonance-frequency dependence of the nuclear spin-lattice relaxation rate $1/T_1$ at elevated temperatures.^{8,9,10,11,12,13)} As to the $S = 1/2$ chain, an analysis of the ω dependence of $1/T_1$ at the Cu site in Sr_2CuO_3 based on the classical spin-diffusion theory gives an unusually high value of the spin-diffusion constant compared with the classical value.¹⁴⁾ This suggests the absence of spin diffusion in the low-temperature limit in consistency with the field-theoretical¹⁾ and perturbative³⁾ approaches. On the other hand, an evidence for diffusive spin transport is found from the proton NMR measurements in $\text{CuCl}_2 \cdot 2\text{NH}_3$ and $\text{Cu}(\text{C}_6\text{H}_5\text{COO})_2 \cdot 3\text{H}_2\text{O}$ at temperatures well above the intrachain exchange interactions.¹¹⁾ Therefore, there seems to be a gap between the high- and low-temperature behavior of the spin transport in the $S = 1/2$ chains, necessitating further experiments on the dynamics, especially on the temperature-dependent properties.

Linear chains of a V^{4+} ion in the compound $\text{-VO}(\text{PO}_3)_2$ may be a model system of an $S = 1/2$ Heisenberg spin chain. $\text{-VO}(\text{PO}_3)_2$ belongs to the monoclinic space group $C2/c$ and has the room-temperature lattice parameters; $a = 15.140$ Å, $b = 4.195$ Å, $c = 9.573$ Å and $\beta = 120.54^\circ$.¹⁵⁾ In the $\text{-VO}(\text{PO}_3)_2$ structure (Fig. 1), VO_5 pyramids are stacked along the b axis to make up a linear chain of V atoms with the nearest-neighbor V-V distance of 4.915 Å. The linear chains are well separated by distorted PO_4 tetrahedra in the a and c di-

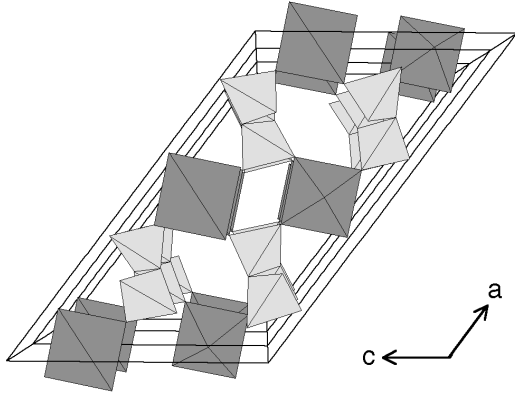


Fig. 1. Crystal structure of $\text{VO}(\text{PO}_3)_2$ viewed from the monoclinic b axis. The dark- and light-shaded polyhedra represent VO_5 pyramids and PO_4 tetrahedra, respectively.

rections, so that good one dimensionality in the b direction is expected. In this paper, we report on the experimental study of the low-frequency spin dynamics in $\text{VO}(\text{PO}_3)_2$ via ^{31}P NMR. The relatively small intrachain coupling ($J=k_B = 3.50$ K estimated from the present susceptibility measurement) in $\text{VO}(\text{PO}_3)_2$ enables us an experimental access to a wide range of temperatures not only $T \sim J=k_B$, where short-range antiferromagnetic correlations are important, but also $T \gg J=k_B$, where electronic spins behave almost paramagnetically. Crossover of the dynamics between the two temperature regimes can also be elucidated by examining the temperature-dependent behavior of, for example, the nuclear spin-lattice relaxation rate. This type of the experiment cannot be done in the canonical $S = 1/2$ Heisenberg antiferromagnetic spin-chain compound Sr_2CuO_3 which has a huge intrachain exchange ($J=k_B = 2200$ K)¹⁶⁾ being suitable for the study of low-temperature dynamics, and will give complementary information for thorough understanding of low-energy spin excitations in the $S = 1/2$ Heisenberg spin chain.

x2. Experiments

Polycrystalline samples of $\text{VO}(\text{PO}_3)_2$ were prepared by a solid-state reaction method. Equimolar mixture of $(\text{VO})_2\text{P}_2\text{O}_7$ and P_2O_5 was fired in an evacuated silica tube at 750 °C for 2 days and at 900 °C for 2 days with the intermediate grinding. $(\text{VO})_2\text{P}_2\text{O}_7$ was prepared as described in ref. 17. The obtained samples were examined by the X-ray diffraction measurement and were confirmed to be a single phase. Magnetic susceptibility was measured using a SQUID magnetometer (Quantum Design MPMS-5s) at 0.1 T. NMR measurements were performed with a standard phase-coherent pulsed spectrometer. ^{31}P NMR spectrum was taken by recording the spin-echo signal with a Box-car averager at a fixed frequency while sweeping the external magnetic field. The nuclear spin-lattice relaxation rate of ^{31}P was measured by a saturation recovery method with a single saturation rf pulse. The measured nuclear magnetization recoveries were single exponential as expected for nuclei with spin 1/2, so that the nuclear spin-lattice relaxation time T_1

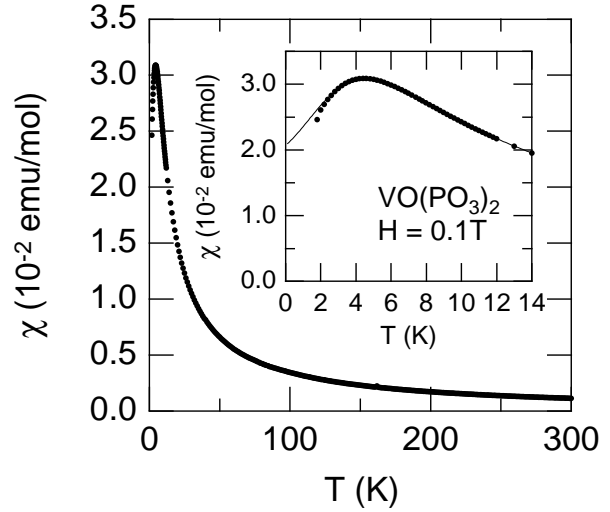


Fig. 2. Temperature dependence of the magnetic susceptibility of $\text{VO}(\text{PO}_3)_2$. The inner core diamagnetic susceptibility (9.2×10^{-5} emu/mol) was subtracted from the raw data. The inset is the expanded view at low temperatures. The solid line in the inset is a fit of the data to the susceptibility of an $S = 1/2$ Heisenberg antiferromagnetic linear chain.

can uniquely be determined as the time constant of the recovery curve.

x3. Results and Analysis

3.1 Magnetic Susceptibility

Figure 2 shows the temperature (T) dependence of the bulk magnetic susceptibility (χ) of $\text{VO}(\text{PO}_3)_2$. While showing Curie-Weiss-like behavior at high temperatures, the susceptibility takes a rounded maximum around $T_{\text{max}} = 4.4$ K as a sign of low-dimensionality of the exchange coupling. The susceptibility can nicely be fitted to the Bonner-Fisher curve for the $S = 1/2$ Heisenberg antiferromagnetic spin chain (HAFC).¹⁸⁾ We estimated the intrachain coupling J between V^{4+} spins by fitting the T dependence of the bulk to the formula;¹⁹⁾

$$\chi = \chi_0 + \frac{N_A g^2 \mu_B^2}{k_B T} \frac{0.25 + 0.14995x + 0.30094x^2}{1 + 1.9862x + 0.68854x^2 + 6.0626x^3} \quad (3.1)$$

Here χ_0 is a T -independent part of χ , N_A is Avogadro's number, g is Landé's g factor, μ_B is the Bohr magneton and $x = J/k_B T$. From the least-squares fit of all the available data points (1.8 to 300 K), we obtained $\chi_0 = 1.05(8) \times 10^{-5}$ emu/mol, $g = 1.978(1)$ and $J=k_B = 3.50(1)$ K. The result of the fit is shown in the inset of Fig. 2. χ_0 may be interpreted as the Van-Vleck orbital paramagnetic susceptibility χ_{VV} , and the obtained value of χ_0 is in a reasonable range for χ_{VV} of a V^{4+} ion. The bulk deviates slightly from the Bonner-Fisher curve below about 2.2 K which may be attributed to the effect of the interchain coupling. As expected, a transition to the long-range ordered state is found to occur at 1.93 K.

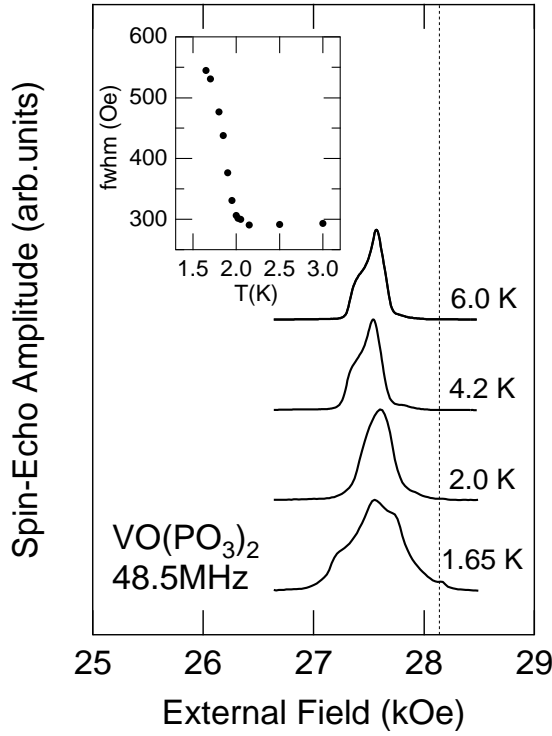


Fig. 3. Temperature variation of the field-swept NMR spectrum of ^{31}P in $\text{VO}(\text{PO}_3)_2$ taken at 48.5 MHz. The dotted line indicates a zero-shift position for ^{31}P . The inset shows the temperature dependence of FWHM of the spectrum.

3.2 NMR spectrum and the Knight shift

Typical examples of the field-swept ^{31}P NMR spectrum are shown in Fig. 3. Above 2.0 K the spectrum exhibits an asymmetric pattern resulting from an axially-symmetric Knight-shift tensor. The spectrum at 2.0 K has some broadening as manifested by smearing of the fine structure which appears at higher temperatures. As the temperature is decreased further, the line becomes broader and exhibits again a characteristic shape with two shoulders on both sides of the peak (except the small one near the zero shift which probably comes from a trace of nonmagnetic impurity phases). The broadening of the spectrum signals the onset of long-range magnetic ordering of V^{4+} spins giving rise to a finite internal magnetic field at the P site. The ordering is considered to be antiferromagnetic because the spectrum is broadened almost symmetrically about its center-of-gravity position in the paramagnetic state. As shown in the inset of Fig. 3, the FWHM of the spectrum exhibits a sudden increase around 2.0 K which gives a rough estimate of the Néel temperature T_N . Indeed, we determined T_N more precisely from the T dependence of the nuclear spin-lattice relaxation rate $1/T_1$ at the P site to be 1.93(1) K where $1/T_1$ is strongly peaked due to critical slowing down of the electronic spins (see Fig. 5).

The NMR spectrum below T_N does not have a rectangular shape which we usually observe for nonmagnetic nuclei in collinear antiferromagnets. The observed line shape, however, can be explained as the one in

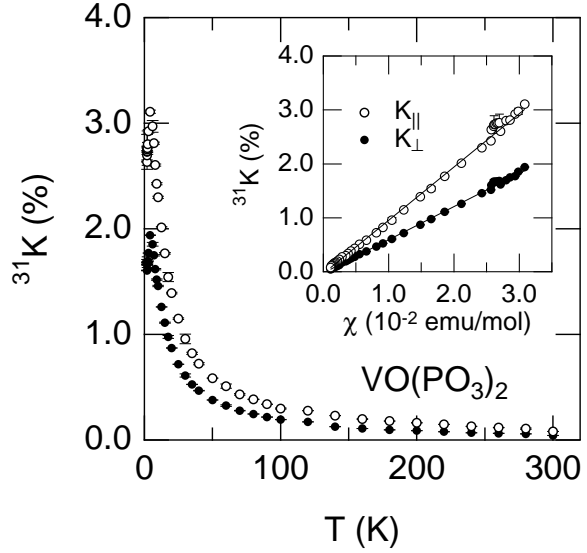


Fig. 4. Temperature dependence of the principal values of the Knight-shift tensor, K_{\parallel} (open circles) and K_{\perp} (solid circles), at the P site in $\text{VO}(\text{PO}_3)_2$. The inset shows the K - χ plot for each principal component. The solid lines in the inset are the linear fit of the data, the slopes of which yield the hyperfine coupling constants A_{\parallel} and A_{\perp} .

the two-sublattice antiferromagnet by taking account of 1) the anisotropy of the hyperfine coupling resulting in the anisotropic Knight-shift tensor in the paramagnetic state, 2) incomplete cancellation of the transferred hyperfine fields from neighboring V^{4+} spins belonging to different sublattices due to the difference of the interatomic distances between V and P atoms, and 3) small tipping in the moment direction from the easy axis under the applied field of which effect is expressed by the parallel and perpendicular susceptibilities. Details of the calculation and the simulation of the spectrum will be given in the appendix, and we only mention here that as shown in Fig. 11 the observed spectrum is well reproduced using physically-reasonable parameters.

From the values of the intrachain coupling J and the Néel temperature T_N , we can estimate the interchain coupling. The interchain coupling J^0 may be evaluated using the expression²⁰⁾

$$\frac{T_N}{J} = \frac{r}{2J} \frac{zJ^0}{J} \quad (3.2)$$

Substituting $T_N = 1.93$ K and $J = k_B \cdot 3.50$ K into eq. (3.2), we obtain $zJ^0/k_B = 2.13$ K. If we disregard for simplicity the difference between the second and third nearest neighbor V-V distances,²¹⁾ $z = 4$ and we get the "average" interchain coupling $J^0/k_B = 0.53$ K (the sign cannot be specified). The ratio $J^0/J = 0.15$ between the intra- and interchain exchange couplings is much larger than those of the other well-known examples of a 1D magnet having J^0/J of order 10^{-2} or less.

A careful analysis of the line shape in the paramagnetic state enables us an independent determination of the principal values of the Knight-shift tensor.²²⁾ We plotted

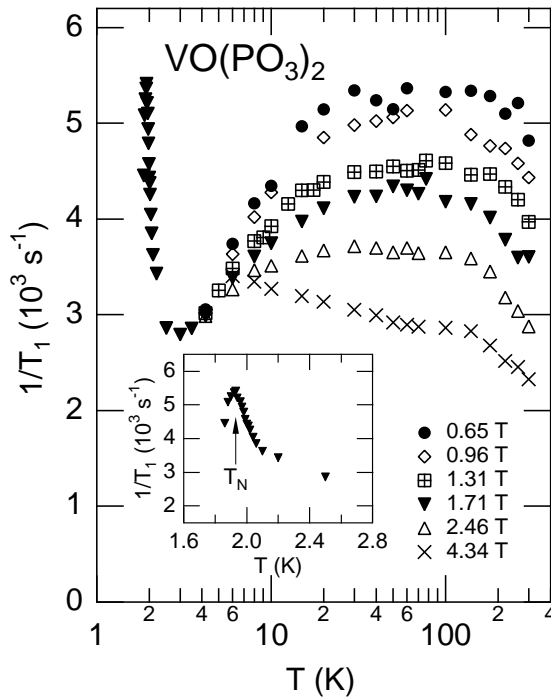


Fig. 5. Temperature dependence of the nuclear spin-lattice relaxation rate at the P site in $\text{VO}(\text{PO}_3)_2$ measured at various magnetic fields. The inset shows the relaxation rate near T_N measured at 1.71 T.

in Fig. 4 the T dependence of the two independent principal components of the Knight-shift tensor, K_k and K_\perp , which correspond to the shift for the magnetic field direction parallel and perpendicular to the symmetry axis at the P site, respectively. The Knight-shift tensor depends strongly on temperature and takes a maximum at 4.2 K as the bulk. As shown in the inset of Fig. 4, both K_k and K_\perp scale with the bulk above and below the susceptibility maximum. From the linear slopes of the K_k and K_\perp versus χ plots, we determined the principal components of the hyperfine tensor at the P site to be $A_k = 5.5(1) \text{ kOe/B}$ and $A_\perp = 3.3(1) \text{ kOe/B}$. These values yield the isotropic and uniaxial components of the hyperfine coupling, $A_{\text{iso}} = (A_k + 2A_\perp)/3 = 4.1(1) \text{ kOe/B}$ and $A_{\text{ax}} = (A_k - A_\perp)/3 = 1.1(1) \text{ kOe/B}$, respectively. The hyperfine coupling at the P site is dominated by an isotropic transferred hyperfine field from the neighboring V^{4+} spins and has a small anisotropic component. A_{ax} is much larger than is expected from the classical dipolar field of the surrounding V^{4+} spins ($\sim 0.18 \text{ kOe/B}$) and may be attributed to polarization of anisotropic p orbitals on the P atom.

3.3 Nuclear spin-lattice relaxation

Figure 5 shows the T dependence of the nuclear spin-lattice relaxation rate $1/T_1$ at the P site under various magnetic fields. The relaxation rate is strongly field dependent and is larger at lower fields. The field dependence becomes weaker as the temperature decreases, and $1/T_1$ becomes almost field-independent at 4.2 K. As

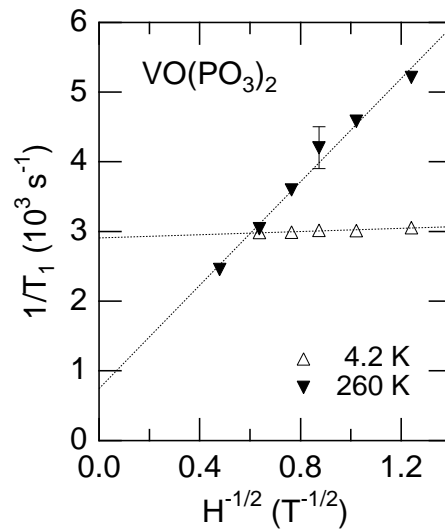


Fig. 6. Nuclear spin-lattice relaxation rate at the P site in $\text{VO}(\text{PO}_3)_2$ as a function of $H^{-1/2}$ at two different temperatures. The dotted lines are the fit of the data to the formula $1/T_1 = P + QH^{-1/2}$.

to the T dependence, $1/T_1$ measured at different fields have some common characteristics. At high temperatures above about 50 K, $1/T_1$ is only weakly T dependent and decreases gradually on increasing temperature. On the other hand, the relaxation rate decreases rapidly below about 50 K except the rate at the field $H = 4.34 \text{ T}$ showing a modest upturn in that temperature region. Note that the decrease of $1/T_1$ at low temperatures is more pronounced at lower fields. Below about 2.5 K, $1/T_1$ exhibits a critical increase toward the long-range magnetic-ordering temperature as shown in the inset of Fig. 5. The maximum of $1/T_1$ is observed at 1.93 K which we determined as the Neel temperature of this compound.

The strong magnetic field (H) dependence of $1/T_1$ is likely to come from spin diffusion characteristic of a low-dimensional Heisenberg spin system. In one dimension the spectral density of the spin-spin correlations diverges as $\omega^{-1/2}$ toward $\omega = 0$ which can be probed as $H^{-1/2}$ dependence of $1/T_1$. Figure 6 shows examples of the H dependence of $1/T_1$ at the P site plotted as a function of $H^{-1/2}$. It is clear that $1/T_1$ obeys an $H^{-1/2}$ law indicating dispersive behavior of the spin-spin correlations. The field dependence can be expressed by the formula $1/T_1 = P + QH^{-1/2}$ where P and Q are fitting constants depending on temperature. While the second term represents the contribution of spin diffusion near $q = 0$, the field-independent term P corresponds to the relaxation rate in the limit $H \rightarrow \infty$ and may be interpreted as a contribution other than spin diffusion like larger- q spin fluctuations. The constant Q is related to spin diffusivity and its magnitude is determined by the spin-diffusion constant (see eq. (3.3) below). Returning to Fig. 6, the dispersive contribution proportional to $H^{-1/2}$ dominates the nuclear-spin relaxation at 260 K. The slope in $H^{-1/2}$ decreases monotonically with decreasing tem-

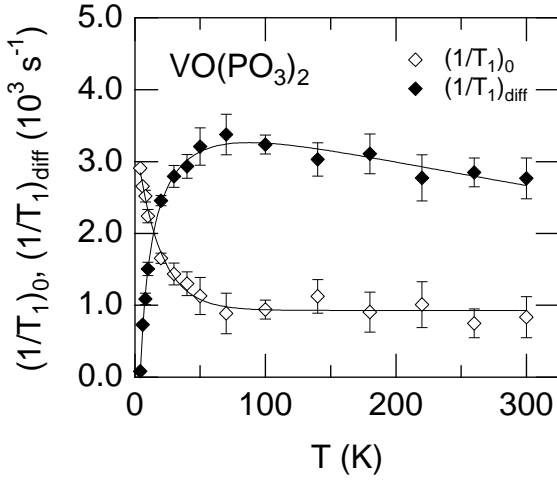


Fig. 7. Temperature dependence of the field-independent relaxation rate $(1/T_1)_0$ (open symbols) and the diffusive contribution $(1/T_1)_{\text{diff}}$ at 1.71 T (solid symbols). The solid lines are guides to the eyes.

perature while the field-independent part of $1/T_1$ grows up. The diffusive contribution vanishes almost entirely at 4.2 K, so that $1/T_1$ is governed by field-independent relaxation processes. Takigawa et al. reported a weak H dependence of $1/T_1$ in Sr_2CuO_3 with a decreasing slope in the $1/T_1$ vs $H^{1/2}$ plot on cooling,¹⁴⁾ similar to the behavior of $1/T_1$ at the P site in $-\text{VO}(\text{PO}_3)_2$ at low temperatures.

The T dependence of the field-independent relaxation rate $(1/T_1)_0$ at P is shown in Fig. 7. $(1/T_1)_0$ is almost T independent with the value of about $1.0 \times 10^3 \text{ s}^{-1}$ above 50 K. This value is somewhat smaller than the calculated value $1/T_{11} = 2.6 \times 10^3 \text{ s}^{-1}$ in the exchange-narrowing limit.²³⁾ Below about 50 K, on the other hand, a substantial increase of $(1/T_1)_0$ was observed. This is contrasted with the behavior of $1/T_1$ in that temperature region where $1/T_1$ decreases rapidly on cooling. The low- T decrease of $1/T_1$ therefore results from the decrease of diffusive contribution which overrides the increasing contribution of $(1/T_1)_0$. It is likely that the increase of $(1/T_1)_0$ at low temperatures is caused by an enhancement of short-range AF correlations within the chain, because geometry at the P site allows intrachain AF spin fluctuations to contribute to the ^{31}P nuclear-spin relaxation.

In Fig. 7 we also showed for comparison the T dependence of diffusive contribution $(1/T_1)_{\text{diff}} = 1/T_1 - (1/T_1)_0$ at 1.71 T. It is clear that, while governing $1/T_1$ at higher temperatures, $(1/T_1)_{\text{diff}}$ decreases rapidly below about 50 K. The decrease of $(1/T_1)_{\text{diff}}$ synchronizes with the increase of $(1/T_1)_0$, which strongly suggests some common origin for them. As mentioned above, the intrachain short-range AF correlation is a likely source for such T -dependent behavior of the nuclear-spin relaxation.

From the slope Q of the $1/T_1$ versus $H^{1/2}$ plot, we can estimate the spin-diffusion constant D_s which de-

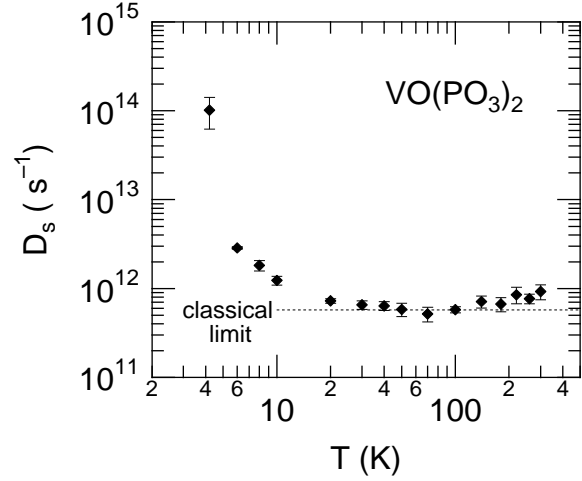


Fig. 8. Temperature dependence of the spin-diffusion constant D_s . The dotted line is a value of D_s in the classical limit.

termines the decay of the spin-spin correlation functions for small q as $\hbar S_q^x(t) S_q^x(0) \sim \exp(-D_s q^2 t) \exp(-i \omega_e t)$ where $\omega_e = g_B H = \hbar$ is the electron Larmor frequency.²⁴⁾ If the hyperfine coupling is predominantly isotropic which is the case for the P site in $-\text{VO}(\text{PO}_3)_2$, a contribution of the longitudinal component of the spectral density of spin fluctuations $S_{zz}(\omega)$ to $1/T_1$ is negligible compared with that of the transverse component $S_{xx}(\omega) = \frac{1}{q} \int_{-1}^1 dt e^{i\omega t} \hbar S_q^x(t) S_q^x(0) g_i$. The nuclear spin-lattice relaxation rate $(1/T_1)_{\text{di}}$ due to spin diffusion is then given as

$$\frac{1}{T_1}_{\text{di}} = \frac{A^2}{\hbar^2} \frac{k_B T}{g^2 \chi_B^2} \frac{\chi_{\text{spin}}}{2D_s \omega_e} \quad (3.3)$$

in one dimension. Here A is the hyperfine coupling constant in units of energy and χ_{spin} is the spin susceptibility per magnetic atom. We determined D_s using the values A_{iso} for A , $\chi_{\text{spin}} = (\chi_0)/N_A$ and g determined from the analysis of the susceptibility and the Knight shift. The result is shown in Fig. 8 where D_s is plotted as a function of temperature. D_s is nearly T independent with the value of $(6-8) \times 10^{11} \text{ s}^{-1}$ above 20 K, while it increases markedly on decreasing temperature. The value of D_s at high temperatures agrees well with the classical limit⁸⁾ $(J = \hbar)^2 S(S+1)/3 = 5/7 \times 10^{11} \text{ s}^{-1}$, which suggests that the spin dynamics is governed by the classical spin diffusion. On the other hand, D_s becomes unusually large below about 10 K compared with the classical value. Such an anomalously large D_s has also been observed in Sr_2CuO_3 ¹⁴⁾ and may be a signature that spin diffusion no longer describes the intrinsic dynamics of the $S = 1/2$ HAFC at low temperatures.

4. Discussion

Although $-\text{VO}(\text{PO}_3)_2$ undergoes a long-range antiferromagnetic transition at $T_N = 1.93 \text{ K}$, the spin dynamics still possesses a one-dimensional (1D) diffusive character at high temperatures as manifested by the strong $H^{1/2}$ dependence of $1/T_1$. On the one hand, a weaker field de-

pendence of $1/T_1$ below about 50 K implies low-energy spin excitations being governed by different physics at lower temperatures. The change of the field-dependent behavior of $1/T_1$ around 50 K is nothing but an evidence for crossover between the two distinct temperature regimes of interest we mentioned in the Introduction, the paramagnetic regime $T > J/k_B$ at temperatures well above the intrachain exchange and the short-range-ordered (SRO) regime $T < J/k_B$ with strong intrachain AF correlations.

In the paramagnetic regime above about 50 K, physical quantities characterizing the dynamics such as $1/T_1$, $(1/T_1)_0$ and D_s are nearly T -independent. $1/T_1$ is governed by 1D dispersive spin excitation near $q = 0$ giving rise to the $H^{-1/2}$ dependence of $1/T_1$ at the P site. On the other hand, the field-independent relaxation rate $(1/T_1)_0$ which may represent the contribution of larger- q spin fluctuations remains small. The spin-diffusion constant D_s in this temperature regime is in good agreement with the value expected in the classical limit, which suggests that the observed dispersive behavior is an intrinsic property of the spin system but not an effect of the coupling with the other degrees of freedom such as phonons.³⁾

As the temperature is decreased below about 50 K, $1/T_1$, $(1/T_1)_0$ and D_s start to vary with temperature. An important observation in this SRO regime is a decreasing contribution of spin diffusion to $1/T_1$. Concurrently with a growth of intrachain AF correlations, dispersive excitations become less important as a possible channel for nuclear-spin relaxation, and at temperatures $T < J/k_B$ where the AF alignment of the spins along the chain is almost established, the dispersive contribution becomes essentially absent. This is characterized by an apparent increase of D_s from the T -independent asymptotic in the paramagnetic regime to a value too large to be explained by the theory of classical spin diffusion. The decrease of dispersive contribution with lowering temperature is considered to be related to the fact that in the low- T limit ($T < J/k_B$) the spin dynamics in the $S = 1/2$ HAFc is not dispersive but purely propagating.²⁾ The apparent increase of D_s in the SRO regime therefore suggests the intrinsic dynamics becoming nondispersive as approaching $T < J/k_B$, and may characterize the crossover to a propagating (ballistic) regime at lower temperatures.

x5. Conclusion

We measured the magnetic susceptibility and the ^{31}P NMR in the compound $-\text{VO}(\text{PO}_3)_2$ as a possible model system of an $S = 1/2$ HAFc. It is found that the susceptibility is well described by the $S = 1/2$ HAFc model with the intrachain coupling $J/k_B = 3.50$ K, although the long-range antiferromagnetic ordering takes place below the Néel temperature $T_N = 1.93$ K.

We observed strong magnetic-field dependence of the nuclear spin-lattice relaxation rate $1/T_1$ at the P site. The field dependence is remarkable at high temperatures ($T > J/k_B$) and is able to be fitted to the form $1/T_1 = P + QH^{-1/2}$ indicating 1D dispersive dynamics of electronic spins. Assuming that the field dependence comes from the 1D spin diffusion, we determined quanti-

tatively the spin-diffusion constant D_s and its T dependence. A good agreement of the observed D_s with the classical value was found at high temperatures, suggesting that dispersive behavior is an intrinsic property of the $S = 1/2$ HAFc in the high-temperature limit.

Contrasted with the field-dependent, diffusion-dominated dynamics at high temperatures, a nearly field-independent $1/T_1$ was observed around $T < J/k_B$. Such a change of the dynamics accompanies an unusual increase of D_s from the classical value as well as a modest increase of the field-independent contribution of $1/T_1$. For the origin we suggested crossover of the intrinsic dynamics to the nondispersive, possibly propagating one due to the intrachain short-range antiferromagnetic correlations. The apparent increase of D_s observed around $T < J/k_B$ characterizes this crossover, and as a consequence of the crossover, the dynamics may smoothly be connected to the one governed by purely propagating, particle-like excitation in the low-temperature limit.

Appendix: Analysis of the NMR line shape in the antiferromagnetic state

The NMR line shape observed in the antiferromagnetic (AF) state is unusual and is to be examined further. We present in this appendix the derivation of the resonance condition appropriate for this specific example and may be applicable if the hyperfine coupling at the nuclear site under consideration has uniaxial symmetry. We also give the calculation of the line shape using the derived resonance condition. From comparison of the calculated spectrum with the observed one, it is shown that the observed line shape is in consistency with collinear antiferromagnetic structure having two sublattices. The point is to take account of an anisotropy of the hyperfine coupling, incomplete cancellation of the transferred hyperfine fields from neighboring magnetic ions, and field-induced canting of sublattice magnetizations.

The resonance frequency ω for nuclei with the nuclear gyromagnetic ratio γ is generally given as

$$\omega = \gamma(H_0 + H_n) \quad (\text{A-1})$$

Here H_0 and H_n are external and internal magnetic fields, respectively. Neglecting the classical dipolar field for the time being, H_n is due to the hyperfine field and is given as

$$H_n = \sum_j \mathbf{A}_{ij} \cdot \mathbf{S}_j \quad (\text{A-2})$$

where \mathbf{S}_j is the electronic spin at the j -th site and \mathbf{A}_{ij} is the hyperfine tensor between the sites i and j .²⁶⁾

In $-\text{VO}(\text{PO}_3)_2$ there are two neighboring V atoms in the distances 3.292 Å and 3.392 Å around the P site and the others are relatively far apart (4.613 Å). Because a transferred hyperfine coupling is generally short-ranged, we may consider a contribution of these two V atoms to H_n at the P site. Labelling these V sites as V(1) and V(2), and similarly the electronic spins as \mathbf{S}_1 and \mathbf{S}_2 , we can rewrite eq. (A-2) as

$$H_n = \mathbf{A}_1 \cdot \mathbf{S}_1 + \mathbf{A}_2 \cdot \mathbf{S}_2 \quad (\text{A-3})$$

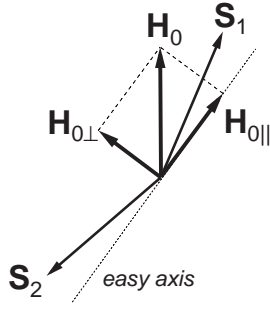


Fig. 9. Schematic view of the canting due to the external field H_0 of the electronic spins S_1 and S_2 . The dotted line indicates the direction of the easy axis. Decomposition of H_0 to the components parallel and perpendicular to the easy axis, H_{0k} and $H_{0\perp}$, respectively, is also shown.

for the P site in $\text{-VO}(\text{PO}_3)_2$. Here \hat{A}_1 and \hat{A}_2 are the hyperfine tensors from V (1) and V (2) sites, respectively. Since V (1) and V (2) belong to the different AF chains, S_1 and S_2 can in principle be either parallel or antiparallel in zero external field.

If S_1 and S_2 are parallel, i.e., V (1) and V (2) belong to the same sublattice, $S_1 = S_2$ and hence $H_n = (\hat{A}_1 + \hat{A}_2) \cdot S$. Because the sum $\hat{A}_1 + \hat{A}_2$ corresponds to the hyperfine tensor in the paramagnetic state, there should be a transferred field of significant magnitude (a few kOe) at the P site. We expect in that case a usual rectangular shape of the spectrum which contradicts with the observation. We therefore assume antiparallel alignment of S_1 and S_2 under zero external field which means that V (1) and V (2) belong to different sublattices.

Under nonzero external field, the sublattice moment changes its direction and magnitude slightly from the zero-field values. If the external field is smaller than the spin- op field, the effect may be expressed by the parallel and perpendicular susceptibilities, χ_k and χ_\perp , in the AF state. It is then convenient to decompose S_1 and S_2 into components parallel and perpendicular to the easy axis for the sublattice moment as $S_j = S_{jk} + S_{j\perp}$ ($j = 1, 2$) and similarly the external field as $H_0 = H_{0k} + H_{0\perp}$ (Fig. 9). The following relations hold between the susceptibilities and the parallel and perpendicular components of S_1 , S_2 and H_0 :

$$S_{1k} + S_{2k} = 2 \chi_k H_{0k}; \quad (\text{A } 4\text{a})$$

$$S_{1\perp} + S_{2\perp} = 2 \chi_\perp H_{0\perp}; \quad (\text{A } 4\text{b})$$

Here χ_k and χ_\perp are defined as the susceptibilities per magnetic atom. Defining $\hat{A} = \hat{A}_1 + \hat{A}_2$ and $\mathbf{a} = \hat{A}_1 - \hat{A}_2$, eq. (A 3) can be written as

$$H_n = \chi_\perp \hat{A} \cdot H_{0\perp} + \chi_k \hat{A} \cdot H_{0k} + \frac{1}{2} [\mathbf{a} \cdot (S_{1\perp} - S_{2\perp}) + \mathbf{a} \cdot (S_{1k} - S_{2k})] \quad (\text{A } 5)$$

$$\chi_\perp \hat{A} \cdot H_{0\perp} + \chi_k \hat{A} \cdot H_{0k} + \mathbf{a} \cdot \mathbf{S}_k; \quad (\text{A } 6)$$

On going from (A 5) to (A 6) we used the approximations $S_{1k} = S_{2k}$ and $S_{1\perp} = S_{2\perp}$. The first and second

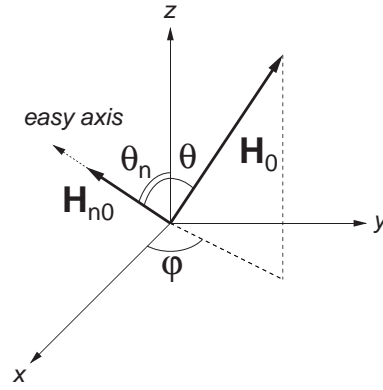


Fig. 10. Principal frame used in the calculation of the resonance frequency. The dotted line with an arrow indicates the direction of the easy axis. The easy axis is taken to be in the zx plane.

terms in eq. (A 6) correspond to the hyperfine field resulting from canting of S_1 and S_2 from the easy axis under nonzero external field. The third term represents the hyperfine field due to the difference between \hat{A}_1 and \hat{A}_2 . Putting $\mathbf{a} \cdot \mathbf{S}_k = H_{n0}$ in eq. (A 6) gives a more convenient form for H_n :

$$H_n = \chi_\perp \hat{A} \cdot H_{0\perp} + \chi_k \hat{A} \cdot H_{0k} + H_{n0}; \quad (\text{A } 7)$$

As has been pointed out, H_{n0} comes from uncancellation of the hyperfine fields from the two neighboring V atoms.

In deriving the expression of the resonance condition from which the line shape is calculated, we take the principal frame of the hyperfine tensor \hat{A} at the P site in which \hat{A} is diagonalized and the principal values are known from the experiment. Taking the z axis as the unique axis of the tensor \hat{A} having axial symmetry, we denote the directions of the easy axis and the external field H_0 by the polar and azimuth angles as shown in Fig. 10. The easy axis can be taken to lie in the zx plane so that $\theta_n = 0$ without loss of generality because of the axial symmetry of \hat{A} . For the field H_{n0} we assume that it is in the direction of the easy axis for simplicity. This is equivalent to neglect the anisotropy of \mathbf{a} . It is noted that with this assumption, the classical dipolar field may be included in H_{n0} so that H_{n0} is regarded as the sum of classical dipolar and hyperfine fields, because the dipolar field is a likely source for the anisotropy field in the $S = 1/2$ system and may be taken to be parallel to the easy axis.

Our aim is to express the resonance frequency ν as a function of the angles θ , θ' and ϕ , and the field strength $H_0 = H_{0j}$ and $H_{n0} = H_{n0j}$. The angles θ and θ' distribute randomly in the polycrystalline sample, resulting in the so-called powder pattern. In the principal frame of \hat{A} , H_0 and H_n are written explicitly as follows;

$$\hat{A} = \begin{pmatrix} A_x & 0 & 0 \\ 0 & A_y & 0 \\ 0 & 0 & A_z \end{pmatrix}, \quad \mathbf{A} = \begin{pmatrix} A_\perp & 0 & 0 \\ 0 & A_\perp & 0 \\ 0 & 0 & A_\parallel \end{pmatrix}; \quad (\text{A } 8\text{a})$$

$$H_0 = \begin{pmatrix} 0 & 1 & 0 \\ b_x H_0 & 0 & 0 \\ b_y H_0 & 0 & 0 \end{pmatrix} \mathbf{A} = \begin{pmatrix} 0 & 1 & 0 \\ H_0 \sin \theta \cos \theta' & 0 & 0 \\ H_0 \sin \theta \sin \theta' & 0 & 0 \end{pmatrix}; \quad (\text{A } 8\text{b})$$

$$H_{n0} = \begin{pmatrix} 0 & 1 & 0 \\ c_x H_{n0} & 0 & A \\ c_z H_{n0} & H_{n0} \cos \theta_n & 0 \end{pmatrix} = \begin{pmatrix} 1 & 0 \\ 0 & A \end{pmatrix} : \quad (A \cdot 8c)$$

A_k and $A_?$ are the principal values of \hat{A} which can be determined from the K - plots in the paramagnetic state. H_{0k} is just the projection of H_0 onto H_{n0} , and hence H_{0k} and $H_{0?}$ can also be written down by components. Substituting eq. (A ·7) into eq. (A ·1) and writing explicitly the components in the principal frame of \hat{A} using eqs. (A ·8), we get after lengthy calculations

$$\omega^2 = \omega_x^2 + \omega_y^2 + \omega_z^2 \quad (A \cdot 9a)$$

with

$$\omega_x = \omega [1 + A_? (c_x^2 k + c_z^2 ?) g b_x + A_? (k - ?) c_x c_z b_z] H_0 + c_x H_{n0};$$

$$\omega_y = (1 + A_? ?) b_y H_0; \quad (A \cdot 9b)$$

$$\omega_z = \omega [1 + A_? (c_z^2 k + c_x^2 ?) g b_z + A_k (k - ?) c_x c_z b_x] H_0 + c_z H_{n0};$$

Note that k ($?$) is not the susceptibility for the z (x ; y) direction(s) in the principal frame of \hat{A} but the one parallel (perpendicular) to the easy axis. Neglecting the terms of $O(A^2)$, and using the relations $b_x^2 + b_y^2 + b_z^2 = 1$ and $c_x^2 + c_z^2 = 1$, eq. (A ·9) can be rewritten as

$$\begin{aligned} \omega^2 = \omega^2 &= H_0^2 + H_{n0}^2 + 2(b_x c_x + b_z c_z) H_0 H_{n0} + 2A_? (c_x^2 k + c_z^2 ?) b_x^2 + A_? ? b_y^2 \\ &+ A_k (c_z^2 k + c_x^2 ?) b_z^2 + (A_k + A_?) (k - ?) b_x b_z c_x c_z H_0^2 + 2A_? (c_x^2 k + c_z^2 ?) b_x c_x \\ &+ A_k (c_z^2 k + c_x^2 ?) b_z c_z + A_k (k - ?) c_z^2 b_x c_x + A_? (k - ?) c_x^2 b_z c_z H_0 H_{n0}; \end{aligned} \quad (A \cdot 10)$$

Equation (A ·10) is valid for arbitrary strength of H_{n0} as far as the conditions A ·1 are satisfied.

If H_{n0} is much larger than A , eq. (A ·10) may be simplified as

$$\omega^2 = \omega^2 = H_0^2 + H_{n0}^2 + 2(b_x c_x + b_z c_z) H_0 H_{n0} \quad (A \cdot 11a)$$

which, by denoting the angle between H_0 and H_{n0} as θ , reduces to

$$\omega^2 = \omega^2 = H_0^2 + H_{n0}^2 + 2H_0 H_{n0} \cos \theta : \quad (A \cdot 11b)$$

Random distribution of θ in the polycrystalline sample yields a usual rectangular shape of the NMR line.²⁵⁾

If H_{n0} is much smaller than H_0 but is comparable with A which is the case here, we may neglect in eq. (A ·10) the terms proportional to H_{n0}^2 or $A H_{n0}$. Hence we arrive at the final expression of the resonance frequency;

$$\begin{aligned} \omega = \omega &= H_0 + [A_? (c_x^2 k + c_z^2 ?) b_x^2 + A_? ? b_y^2 + A_k (c_z^2 k + c_x^2 ?) b_z^2 \\ &+ (A_k + A_?) (k - ?) b_x b_z c_x c_z] H_0 + (b_x c_x + b_z c_z) H_{n0}; \end{aligned} \quad (A \cdot 12)$$

or writing explicitly the dependence on the angles as

$$\begin{aligned} \omega = \omega &= H_0 + [A_? (k \sin^2 \theta_n + ? \cos^2 \theta_n) \sin^2 \theta \cos^2 \theta' + A_? ? \sin^2 \theta \sin^2 \theta' \\ &+ A_k (k \cos^2 \theta_n + ? \sin^2 \theta_n) \cos^2 \theta + \frac{1}{4} (A_k + A_?) (k - ?) \sin 2 \theta_n \sin 2 \theta \cos \theta'] H_0 \\ &+ (\sin \theta_n \sin \theta \cos \theta' + \cos \theta_n \cos \theta) H_{n0}; \end{aligned} \quad (A \cdot 13)$$

For the field-sweep measurement the resonance frequency ω is fixed while the external field H_0 is varied. It is therefore necessary to solve eq. (A ·14) with respect to H_0 , the result of which is not given here explicitly because it is rather straightforward. Then we calculate the spectrum $f(H_0) / N = H_0$ by counting the number of nuclei N having the resonance field between H_0 and $H_0 + \Delta H_0$. More than million different (θ ; θ') points representing the random distribution of H_0 were taken to calculate the resonance field. The unknowns H_{n0} , θ_n , k and $?$ in (A ·14) are treated as parameters to reproduce

the observed spectrum. As shown in Fig. 11, an appropriate choice of the parameter values reproduces the observed two-shoulder structure of the spectrum in the AF state. We may therefore conclude that the magnetic ordering in $\text{-VO}(\text{PO}_3)_2$ is not unusual but is rather conventional.

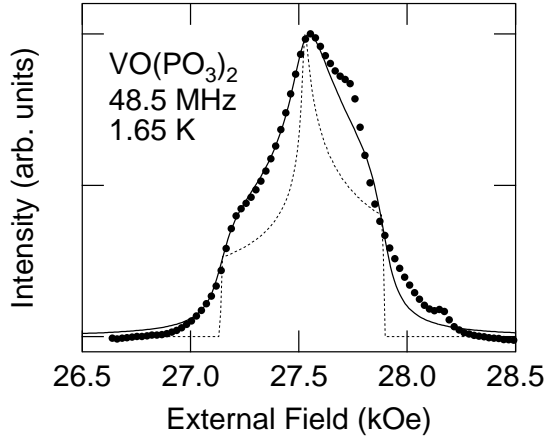


Fig. 11. Comparison of the calculated powder patterns with the observed spectrum at 1.65 K. The solid circles represent the experimental data. The dashed line is the calculated spectrum $f(H_0)$ with no inhomogeneous broadening. The parameters used in the calculation are $\nu = 48.5$ MHz, $A_k = 5.5$ kOe/B, $A_z = 3.3$ kOe/B, $H_{n0} = 310$ Oe, $n = 33$, $\gamma_k = 0.026$ emu/mol and $\gamma_z = 0.031$ emu/mol. The spectrum shown by the solid line is calculated by taking account of inhomogeneous distribution of the internal field H_{n0} . The effect is introduced by convoluting Lorentzian with the FWHM of 55 Oe.

[23] T. Moriya: Prog. Theor. Phys. 16 (1954) 641.

[24] The power law decay of the spin autocorrelation function $\langle S_i^x(t) S_i^x(0) \rangle / t^{-1/2}$ (eq. (1.1)) can be derived by integrating $\langle S_i^x(t) S_i^x(0) \rangle$ over q in one dimensional space.

[25] J. Kikuchi, K. Ishiguchi, K. Motoya, M. Itoh, K. Inari, N. Eguchi and J. Akimitsu: J. Phys. Soc. Jpn. 69 (2000) 2660.

[26] S_j fluctuates in time and hence H_n in eq. (A.1) should be the time average because we are dealing with the resonance frequency. For simplicity of notation we omit the brackets here to show explicitly the time-averaging procedure and use S_j and H_n as the time-averaged quantities.

-
- [1] P. G. de Gennes: Magnetism, ed. G. T. Rado and H. Suhl (Academic Press, New York, 1963) Vol. III, p. 115.
- [2] S. Sachdev: Phys. Rev. B 50 (1994) 13006.
- [3] B. N. Narozhny: Phys. Rev. B 54 (1996) 3311.
- [4] K. Fabricius and B. M. McCoy: Phys. Rev. B 57 (1998) 8430.
- [5] F. Naef and X. Zotos: J. Phys.: Condens. Matter 10 (1998) L183.
- [6] B. N. Narozhny, A. J. Millis and N. Andrei: Phys. Rev. B 58 (1998) R2921.
- [7] X. Zotos: Phys. Rev. Lett. 82 (1999) 1764.
- [8] D. Hone, C. Scherer and F. Borsa: Phys. Rev. B 9 (1974) 965.
- [9] F. Borsa and M. Mali: Phys. Rev. B 9 (1974) 2215.
- [10] Y. Barhoux, J.-P. Boucher and J. Karra: Physica 86-88 B (1977) 1307.
- [11] Y. Ajiro, Y. Nakajima, Y. Furukawa and H. Kiriya: J. Phys. Soc. Jpn. 44 (1978) 420.
- [12] M. Takigawa, T. Asano, Y. Ajiro, M. Mekata and Y. J. Uemura: Phys. Rev. Lett. 76 (1996) 2173.
- [13] J. Kikuchi, T. Yamachi and Y. Ueda: J. Phys. Soc. Jpn. 66 (1997) 1622.
- [14] M. Takigawa, N. Motoyama, H. Eisaki and S. Uchida: Phys. Rev. Lett. 76 (1996) 4612.
- [15] E. B. Murashova: Kristallografiya KRISA 39 (1994) 145.
- [16] N. Motoyama, H. Eisaki and S. Uchida: Phys. Rev. Lett. 76 (1994) 3212.
- [17] J. Kikuchi, K. Motoya, T. Yamachi and Y. Ueda: Phys. Rev. B 60 (1999) 6731.
- [18] J. C. Bonner and M. E. Fisher: Phys. Rev. 135 (1064) A 640.
- [19] W. E. Hatfield: J. Appl. Phys. 52 (1981) 1985.
- [20] J. Kondo: Physica B 123 (1984) 169.
- [21] The second and third nearest neighbor V atoms are in the distances of 5.223 Å and 6.092 Å at room temperature.
- [22] A. Abragam: Principles of Nuclear Magnetism (Oxford University Press, Oxford, 1961).